Projectile velocity and target temperature dependence of charge-state distributions of multicharged ions scattered during grazing interactions with a Au(110) surface

Q. Yan, D. M. Zehner, and F. W. Meyer
Oak Ridge National Laboratory, Oak Ridge, Tennessee 37831-6372

S. Schippers
Kernfysisch Versneller Institute, Zernikelaan 25, NL 9747 AA Groningen, The Netherlands

(Received 15 February 1996)

We have made systematic measurements of scattered projectile charge-state distributions for multicharged He, N, Ne, Na, and Ar ions grazingly incident on a Au(110) single-crystal target. For projectiles whose neutral binding energies lie below the valence band (N, Ar, He, and Ne), observed 1+ charge fractions were small at low velocities and steeply increased above well-defined threshold velocities. However, for Na projectiles with neutral binding energy above the Fermi level, a large (about 84%) 1+ charge fraction was found. The velocity dependence of the Na neutral fraction shows a ''kinematic resonance'' due to the virtual population of electronic states above the Fermi level in the projectile rest frame. The measured sample temperature dependence of the scattered 1+ charge fraction for Ne^{9+} projectiles incident along the [110] surface channeling direction reveals a significant decrease in projectile neutralization once the (2×1)-(1×1) phase transition temperature of the Au(110) surface at 650 K has been reached. [S1050-2947(96)07207-1]

PACS number(s): 34.50.Dy, 34.70.+e, 79.20.Rf, 79.90.+b

I. INTRODUCTION

The study of the interaction of slow multiply charged ions with surfaces has developed into a very active field of research within the general area of particle-solid interactions. Most experimental work to date in this area has focused on measurement of x-ray [1] and electron [2–6] emission, as well as scattered ion angular distributions resulting from grazing surface interactions of highly charged ions [7,8]. Characteristic shifts of the scattered ion angular distributions away from the specular reflection angle have been observed, and were attributed to image charge acceleration [9] of the highly charged ion during its approach to the surface. The extent of these shifts provided direct evidence of a stepwise neutralization of the multicharged ion during its approach to the surface. Recently we have reported on measurements [8,10,12] of the charge-state distributions of multicharged ions scattered during grazing surface collisions, which have provided additional insights into the question of projectile neutralization. Experimental data on charge-state distributions resulting from surface channeling interaction of 3.75 keV/amu O^{q+} $(3\leqslant q\leqslant 8)$ ions with Au(110) have shown that the scattered projectile charge-state distributions are largely independent of incident charge [10]. Similar charge equilibration effects have been observed for singly charged incident ions by Närmann *et al.* [11]. Simulations of the ion trajectory indicated that the projectile spends less than 30 fs within 2 Å of the topmost Au surface layer [10,12]. This very fast equilibration time was a strong experimental indication that, already at the target interface (i.e., the topmost lattice plane), strong screening, essentially characteristic of the bulk, is established that facilitates direct capture to projectile inner shells. Theoretical results [9] for the neutralization and relaxation of multicharged O^{q+} ions using the classical over-the-barrier model (COB) and incorporating screening effects on projectile energy levels reproduce the major features of the measured charge distributions, and support the above conclusion. Both experiment and simulations [9,10] suggest, furthermore, that interactions on the approach trajectory have almost no affect on the final charge-state distribution of the projectiles. Moreover, in the low keV/amu energy range investigated, the scattered projectiles appear to have lost memory of their original charge state, and the final distribution of dominant charge states is almost exclusively determined by interactions of the scattered projectiles as they leave the surface.

In the present investigation, scattered ion charge-state distributions resulting from interactions with Au(110) are explored in greater detail. In particular, measurements are reported for a range of different projectile species and charge states covering a broad range of energies that extends up to our maximum attainable energies of $\sim q\times 20$ keV, where q is the ionic charge. The lowest investigated energies extended down to $\sim q\times 0.8$ keV, which are still significantly above the few tens of eV regime where trajectory-dependent neutralization has recently been found [13]. As has been pointed out previously [9], the COB model is not suited to treat electron capture of very low charge-state ions, and therefore, may not give adequate insight into the final phase of projectile neutralization. The present measurements explore this stage of the neutralization process in a systematic way by monitoring the dominant scattered ion charge fractions (in the present case, +1 and neutral atoms) and determining their dependence on projectile velocity and on the binding energy of the last electron captured during the course of the projectile neutralization. In addition, the effect of surface order on projectile neutralization is explored by measurements of charge-state distributions as a function of the Au(110) target temperature. The reported measurements were carried out using a two-dimensional position-sensitive detector (PSD), which permits detection of all possible scattered charge states (i.e., positive ions, neutral atoms, as well as negative

ions), making possible the extraction of absolute scattered projectile charge fractions. The velocity-dependence measurements were performed under surface-channeling [14] conditions, as verified by observation of characteristic angular distributions for the reflected projectiles, in order to assure minimal penetration of the target surface plane and well-defined projectile trajectories.

II. EXPERIMENTAL APPROACH

In the present experiment multicharged ions, produced by a CAPRICE ECR ion source [15] at the Oak Ridge National Laboratory Multicharged Ion Research Facility, are grazingly incident (about 1.5°) on a clean Au(110) surface. The incident multicharged ion beam is collimated by two 0.5-mm-diam apertures to an angular divergence of about 0.1° full width at half maximum (FWHM). The scattering geometry has been described previously [10]. The single-crystal Au(110) target is mounted on an x-y-z manipulator located in an ultra-high-vacuum (UHV) chamber having a base pressure of 3×10^{-10} mbar and is prepared by cycles of surface sputter cleaning with 1-keV Ar^+ ions and crystal annealing at about 700 °C. The heating of the sample is accomplished by a button heater and the temperature of the sample is monitored by a nickel-chromium thermocouple secured in a small hole located near one of the edges of the Au target. Surface cleanliness is verified using electron-induced Auger electron spectroscopy. Both the angular distribution (polar as well as lateral) and the charge-state distribution of the scattered (reflected) projectiles were measured using a two-dimensional position-sensitive detector (PSD) (Quantar Technology Model 3394A) having a 40-mm-diam active area. Moveable slits located between the target and the PSD were completely opened for measurements of angular scattering distributions. For the charge-state distribution measurements they were closed symmetrically about the ion beam to select a thin vertical slice of the scattered beam, which was then dispersed by charge state across the face of the PSD using a pair of electrostatic deflection plates located immediately downstream of the slit assembly. The target-PSD distance is about 560 mm. The PSD is mounted on a second x-y-z manipulator, which permits measurement of the polar scattering angle ϕ_p in the range $-0.8°$ to $+5.6°$. The position of the primary beam, used to determine $\phi_p=0°$, as well as its angular spread, can thus be directly measured. In order to avoid saturation of the PSD, beam intensities on target were kept sufficiently low that the total scattered ion flux on the PSD did not exceed 100 kHz. The errors associated with the charge fraction measurements were due to a slight nonuniform response of the active area of the PSD, and a charge-state-dependent detection efficiency of the detector in the low-energy region. For the Na, N, and Ar projectiles, the combination of these effects resulted in an estimated error not exceeding 10%. As will be discussed below, for the Ne and He projectiles, differences in the efficiencies for detecting neutral and singly-charged projectiles may be significantly larger at the lowest energies investigated, resulting in correspondingly larger uncertainties for the latter projectiles.

III. VELOCITY-DEPENDENCE MEASUREMENTS

In the following three sections charge fraction velocity dependences will be presented for incident projectile species

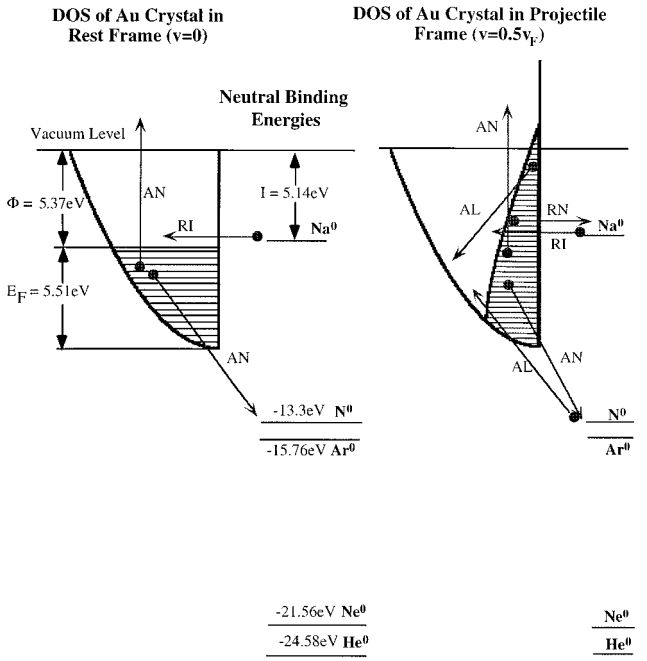

FIG. 1. Schematic energy-level diagrams of a Au(110) and ground states of Na, N, Ar, Ne, and He atoms.

of varying neutral binding energies, starting from slightly above the Fermi energy of Au(110) (Na projectiles), to a few eV below the bottom of the valence band of Au(110) (N and Ar projectiles), and finally to about 10 eV below the bottom of the valence band (He and Ne projectiles). As will be seen below, a strong correlation is observed between the magnitudes of the neutral and 1+ charge fractions and the neutral binding energies of the various projectiles. For future reference, a schematic energy-level diagram of the Au(110) target valence band and the unshifted ground states of the investigated Na, N, Ar, Ne, and He projectiles is shown in Fig. 1. For reasons that will become apparent in Sec. IV, during the measurements summarized below, the Au(110) target was kept at a constant elevated temperature of about 450 K.

A. Na ions incident on Au(110)

The projectile velocity dependence of the scattered neutral fraction for sodium ions incident on Au(110) is shown in Fig. 2. The measured neutral fractions for projectiles with the same velocity but different initial charge states were found to vary by less than 5%. This result allowed us to determine equilibrium scattered ion charge-state distributions over a wide range of velocities by using multicharged ions up to Na^{9+}. The measurements covered the velocity range of 0.12 to 0.56 a.u. The neutral fraction was measured to be very small at low velocities, increased with increasing velocity up to a maximum value of about 16% at a velocity around 0.3 a.u. and then decreased again at yet higher velocity. The velocity dependence thus displays a characteristic ''kinematic resonance'' shape, similar to that seen in earlier measurements of K incident on Al(111) by Zimny *et al.* [16].

''Kinematic resonance'' effects [17,18] are operative in the case of projectiles having nonzero parallel velocity components with respect to the target surface. In the rest frame of

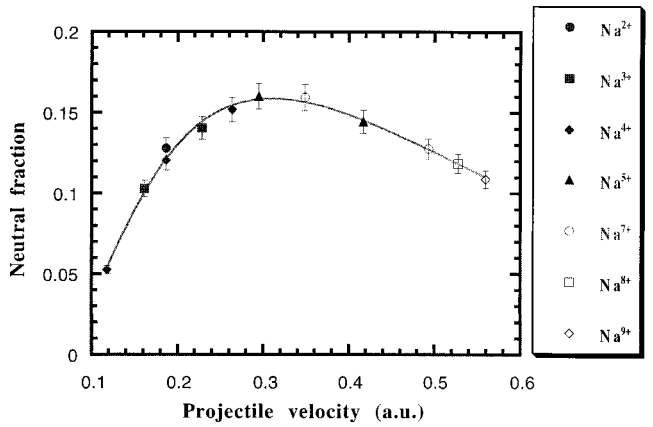

FIG. 2. The projectile velocity dependence of the scattered neutral fraction for sodium ions incident on Au(110) along the [110] direction. The solid lines are fitting curve based on Eq. (1). The fitting of data gives the ''energy gap'' of 1.28 ± 0.05 eV and ''characteristic velocity'' of 0.130 ± 0.004 (in atomic units).

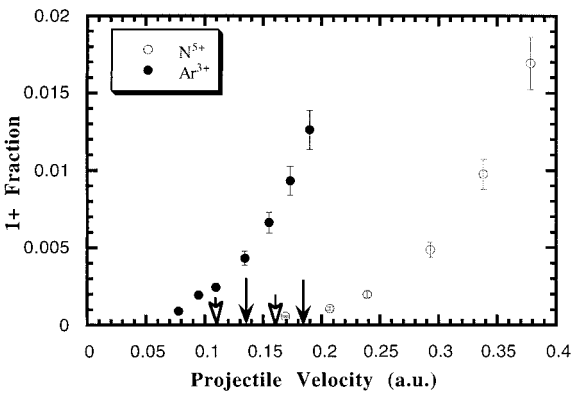

FIG. 3. The projectile velocity dependence of the scattered 1+ charge fraction for incident N^{5+} (open circles) and Ar^{3+} (solid circles) on Au(110) along the [110] direction. Two solid arrows indicate threshold velocities for the Ar projectile at 0.136 and 0.186 a.u. corresponding to formation distances of 1 and 3 Å, respectively. Two open arrows show the threshold velocities for the N projectile at 0.11 and 0.16 a.u. for formation distances of 1 and 3 Å, respectively (see text).

such projectiles, a modification of the Fermi-Dirac distribution of target electrons results in a population of occupied electronic states above the Fermi edge. The neutral binding energy of Na is 5.14 eV and this level is shifted upwards with decreasing distance to the surface due to the image charge interaction. As seen in Fig. 1, the Fermi level of Au(110) is 5.37 eV below the vacuum level. If the projectile has zero parallel velocity, only resonance ionization is possible when the Na atom is close to the Au(110) surface. In this case, almost 100% of backscattered projectiles will be singly charged. However, if the parallel velocity is high enough, occupied states of the solid can come into resonance with a projectile whose neutral binding energy is less than the surface work function of the target. As a result, resonance neutralization becomes possible. The resulting neutral fraction reflects the density of occupied states of metal target electrons at the shifted atomic level ''seen by'' the moving projectile. The density of states goes through a maximum as a function of projectile velocity, which is seen as well in the neutral fraction of scattered projectiles. This so-called ''kinematic resonance'' shape of the scattered projectile neutral fraction is well described by the following analytic expression [17,19]:

$$P_0 \approx \frac{1}{1+\frac{g^-}{g^+}\exp\left[\frac{E_g(y_s)+v^2/2}{v_c v}\right]}, \tag{1}$$

where g^- and g^+ are factors taking into account the degeneracies of the initial and final atomic levels. For the case of the sodium projectile, $g^+=2$ and $g^-=1$. The product vv_c represents the virtual ''motional'' temperature [19] characterizing the Fermi-Dirac distribution of the target conduction band in the rest frame of the moving projectile. In what follows, the ''characteristic velocity'' v_c is treated as a fitting parameter, since its *a priori* calculation is beyond the scope of the present work. E_g is called the ''energy gap'' between the Fermi level and the shifted atomic level and is given by the following equation:

$$E_g = \Phi - |E_a + \Delta E_a|, \tag{2}$$

where Φ is the work function of the surface, E_a is the neutral binding energy of the projectile, and $\Delta E_a \approx (2q+1)/4z$ is the image shift [9] of the atomic level, with z the distance above the surface image plane (both energy shift and distance in atomic units), and q the projectile charge (i.e., 0 for a neutral atom).

The curve in Fig. 2 represents a best fit according to Eq. (1), giving an ''energy gap'' E_g of 1.28 ± 0.05 eV and a ''characteristic velocity'' v_c of 0.130 ± 0.004 a.u. The work function of Au(110) is 5.37 eV. Since the neutral binding energy of sodium is 5.1 eV, based on Eq. (2) the sodium level is shifted by 1.01 eV, corresponding to a distance of formation above the image plane of $\sim 6.7a_0$. The final step of the charge equilibration is thus a competition between resonant ionization and neutralization when the scattered Na projectile is still within ~ 3 Å above the actual surface plane, in agreement with our earlier estimates [10].

B. N and Ar ions incident on Au(110)

Figure 3 shows the scattered 1+ charge fraction as a function of velocity for incident N^{5+} and Ar^{3+} on Au(110)along the [110] surface channeling direction. Unlike the case of Na projectile impact on the surface, at the lowest investigated energies, the neutral fraction is found to dominate for incident N and Ar projectiles. On the linear plot used for Fig. 3, the 1+ charge fractions for both species are seen to exhibit threshold behaviors, and increase steeply above characteristic velocities specific to each projectile.

Referring to Fig. 1, the bottom of the Au valence band (V) is 10.88 eV ($V=E_F+\Phi$, Fermi energy $E_F=5.51$ eV; $\Phi=5.37$ eV) below the vacuum level. The neutral ground-state binding energies of nitrogen and argon are 14.5 and 15.76 eV, respectively. Since these levels are about 5 or 6 eV below the bottom of the valence band, and the first excited levels are significantly above the top of the band, electron

transfer through Auger processes [20], involving two electrons, will most likely be dominant in determining the final charge state of these scattered projectiles. For zero projectile velocity, Auger neutralization would be the only possible process and an almost 100% neutral fraction would be expected. However, above a certain threshold velocity, Auger loss can occur in the projectile rest frame such that an electron in a low atomic level can transfer up to an unoccupied state of the solid while another electron in a high occupied state moves down to a low unoccupied state of the solid, resulting in projectile ionization. A schematic representation of this process is shown in Fig. 1. The threshold velocity for this process can be written from conservation of energy considerations as follows [21]:

$$v_{\mathrm{th}}=3v_F\left(1-\sqrt{1+\frac{(\Phi-I^*)}{9E_F}}\right), \tag{3}$$

where v_F is the Fermi velocity of Au(110) and $I^*=E_a+\Delta E_a$ is the binding energy of the shifted projectile level. Despite initial appearances, direct determination of threshold velocities from the velocity dependence of the charge fractions is somewhat arbitrary. Instead, we show in Fig. 3 theoretical threshold velocities determined for each projectile from Eq. (3), assuming two different above-surface formation distances, 3 Å and 1 Å. The larger distance is the maximum above-surface distance inferred for resonant processes, while the smaller is expected to be more representative for Auger-type processes, such as the one discussed above. As can be seen from the figure, the 1+ charge fraction velocity dependence for the Ar projectiles is consistent with a very small above-surface formation distance, as is expected for an Auger-type process. The onset of the rise of the 1+ fraction for N projectiles appears to be somewhat delayed relative to the calculated threshold values. It is noted, however, that the 1+ fraction is already finite (i.e., not zero) at the lowest measured velocity of 0.17 a.u. Furthermore, we cannot eliminate the possibility that the Auger loss rates for Ar and N projectiles may be different due to differences in the neutral ground-state wave functions for these two species.

It is of course also possible that, instead of reflecting the opening of a loss channel, the rise of the 1+ fractions beyond their respective velocity thresholds is due to incomplete neutralization as the interaction time becomes less than the characteristic Auger neutralization time. Within this scenario, however, it would appear difficult to explain the almost exponential rise of the 1+ fractions beyond the velocity threshold.

C. Ne and He ions incident on Au(110)

The velocity dependences of the scattered 1+ charge fraction for incident Ne^{q+} ($q=1$, 2, 3, 4, and 8) and He^{2+} on Au(110) along the [110] surface channeling direction are shown in Fig. 4. The 1+ charge fractions were found to be small but finite at very low velocity and to increase steeply beyond characteristic threshold velocities in a similar fashion as the N and Ar projectiles. The scattered 1+ fractions for the Ne^{q+} projectiles with the same velocity but different charge state were found to differ by less than 10%. This

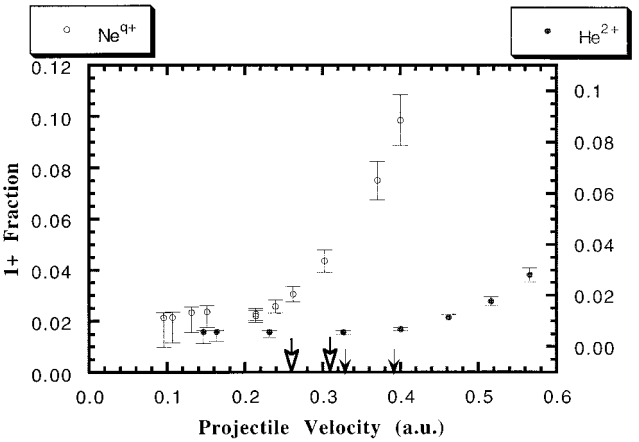

FIG. 4. The projectile velocity dependence of the scattered 1+ charge fraction for incident Ne^{q+} ($q=1$, 2, 3, 4, and 8, open circles) and He^{2+} (solid circles) on Au(110) along the [110] direction. The right two arrows (solid arrows) indicate threshold velocities for the He projectile at 0.33 and 0.39 a.u. for formation distances of 1 and 3 Å, respectively. The left two arrows (open arrows) show threshold velocities for the Ne projectile at 0.26 and 0.31 a.u. for formation distances of 1 and 3 Å, respectively (see text).

result again demonstrates that the scattered projectile charge-state distributions are almost completely equilibrated.

As seen from Fig. 1, the neutral binding energy of neon and helium is 21.56 eV and 24.59 eV, respectively, which is far below the bottom of the valence band of Au(110). The final charge-state distribution of scattered projectiles is likely still determined by Auger processes. Proceeding in the same manner as outlined in Sec. III B, we show in Fig. 4 the two different calculated threshold velocities for each projectile. As is evident by comparison with the measurements, the velocity dependences of the 1+ charge fractions for both species is again consistent with the very small formation distances at which the probability for Auger processes is expected to maximize.

It remains to comment on the finite 1+ charge fraction plateaus evident in Fig. 4 for both the Ne and He projectiles at the lowest investigated energies. There are at least two possible explanations for these features in the data. The first assumes that the presence of the plateaus for these two projectiles reflects the presence of additional ionization channels that were absent for the N and Ar projectiles. Since for both He and Ne projectiles (unlike the N and Ar projectiles) there exist neutral excited states close in energy to the top of the metal valence band, it is possible that the plateaus result from resonance ionization of such states formed by resonant capture at larger distances, which are subsequently shifted above the Au target Fermi level by image and screening effects [9] as the distance to the surface decreases. In general, the relaxation of these projectile excited states will occur as a competition between the above resonance ionization and Auger deexcitation. Since the neutral ground states of both He and Ne lie far below the bottom of the conduction band of Au(110), the corresponding Auger deexcitation rates are expected to be small, leading to the ultimate loss of the excited electron in both instances to the metal conduction band, and an incompletely neutralized scattered projectile. In this scenario it would then appear that the finite low-energy

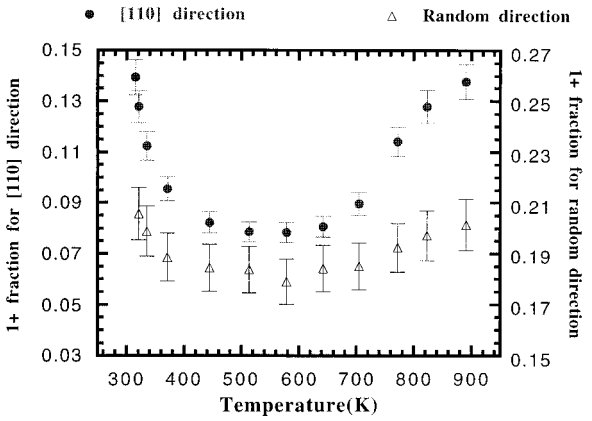

FIG. 5. Temperature dependence of the scattered 1+ charge fraction for 72-keV Ne^{9+} projectiles grazingly incident along the [110] direction (solid circles) and a random direction (open triangles) of the Au(110) surface.

1+ plateaus observed for He and Ne projectiles are a last vestige of the initial ''hollow-atom'' formation on their approach to the surface.

It is, however, also possible that the observed plateaus are artifacts created by progressively larger differences in detection efficiencies between +1 ions and neutral atoms for the two species in question as the projectile energy is decreased into the low keV range. Secondary electron emission measurements for He and Ne singly charged and neutral projectiles incident on Mo have shown [22] that the secondary electron coefficients γ are much less than unity below 5–10 keV, and, moreover, that the γ for neutral atoms are significantly smaller than those for 1+ ions (over the same energy range, such differences are much less pronounced for N and Ar projectiles). Since particle detector efficiencies are typically proportional to the probability with which the incident projectile ejects at least one electron (given by $1-e^{-\gamma}$ under the assumption of Poisson statistics [23]), these differences in γ can result in a significant charge dependence of the channelplate detection efficiencies at very low energies. In the absence of explicit measurements for our detector, we have assumed that the measurements for Mo are applicable to channelplates, and have calculated the effect that the deduced response difference for 1+ and neutral impact has on our low-energy He and Ne data, indicated as the lower extremes of the error bars shown in Fig. 4. As is evident from the figure, for the Ne projectiles maximum downward corrections of a factor of 2 were estimated, while for the He projectiles, the maximum estimated effect exceeded a factor of 5 decrease at the lowest energy.

IV. TARGET TEMPERATURE-DEPENDENCE MEASUREMENT

In order to follow up an earlier noted observation [12] of a significant variation of the scattered ion charge fractions with time elapsed subsequent to sample annealing, we also investigated the dependence of the measured charge distributions on sample temperature. Figure 5 shows the temperature dependences of the scattered 1+ charge fraction for 72-keV Ne^{9+} projectiles grazingly incident both along the [110] direction and a random direction of the Au(110) surface. The sequence was started at the annealing temperature around 950 K after cycles of surface sputtering and annealing. Each charge-state distribution measurement was carried out at a temperature held constant to within a few degrees. From a value of 14% at 900 K, the 1+ fraction for projectiles incident along the [110] direction was observed to decrease to about 8% around 650 K. The scattered 1+ charge fraction was almost independent of sample temperature in the range 650–450 K. The temperature dependence of the scattered 1+ charge fraction for projectiles incident along a random direction of the Au(110) surface is much weaker over the same temperature range. Below 450 K the 1+ charge fractions increase again.

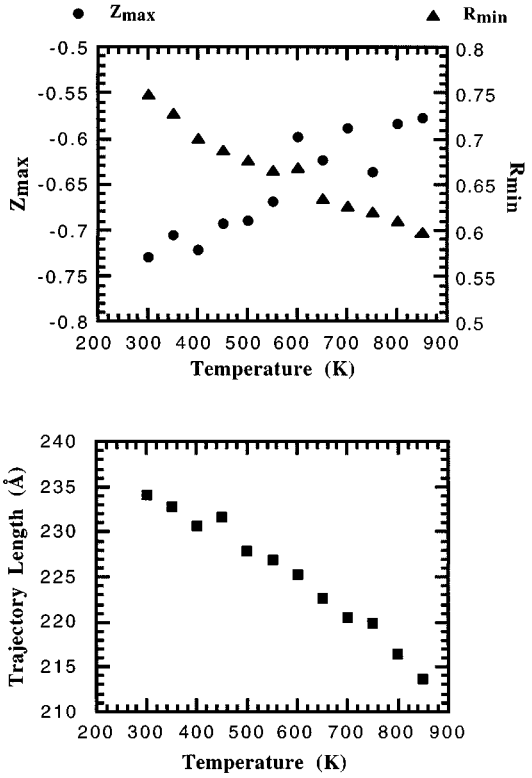

FIG. 6. Top: simulation results for the temperature dependencies of the binary collision minimum distance of closest approach (R_{min}), the maximum penetration depth (Z_{max}) in the case of 72-keV Ne^{9+} projectiles grazingly incident along the [110] direction at 1.5° on Au(110). Bottom: simulation results for the total trajectory length within 2 Å of the topmost Au surface layer under the same incidence condition.

In order to understand the influence of temperature on the trajectories along which the projectiles travel under the condition of surface channeling, a Monte Carlo simulation was carried out in which the equations of motion of the projectile in the periodic potential of the crystal surface were solved for an ensemble of appropriate random initial conditions [10,12]. The scattering potential consisted of a superposition of individual contributions [assuming a Ziegler-Biersack-Littmark (ZBL) interaction potential] from a lattice cell of 72 atoms that was progressively translated along the ion trajectory. Lattice vibrations were accounted for by employing the Debye model with an anisotropic surface Debye temperature

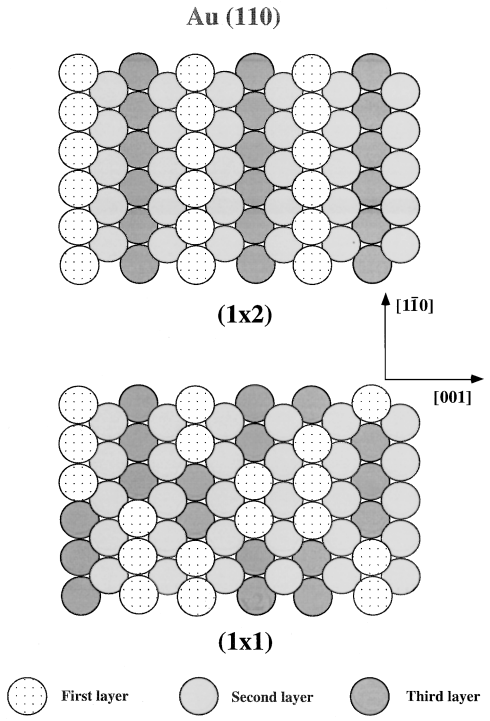

FIG. 7. Top view of the (2×1) surface reconstruction and the random (1×1) surface phase of Au(110) above 650 K.

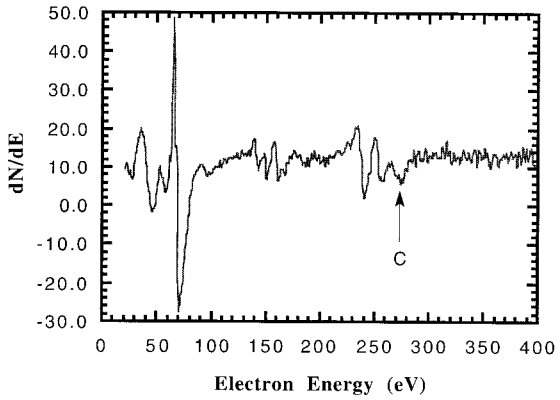

FIG. 8. Auger electron spectrum of the Au(110) surface after cooling down to room temperature (3 h after annealing).

[10]. Figure 6 shows the simulation results for the temperature dependences of the binary collision minimum distances of closest approach (R_{min}), the maximum penetration depths (Z_{max}), and the total trajectory lengths within 2 Å of the topmost Au surface layer for the case of 72-keV Ne^{9+} projectiles grazingly incident at 1.5° on the Au(110). With these three parameters, the surface interaction leading to the observed charge-state distribution is essentially defined. The simulation studies show a smooth change of all these parameters with changing temperature. In contrast, the experimental results on the scattered 1+ charge fraction show an abrupt increase with temperature beyond 650 K. Therefore, increased thermal lattice vibration with increased sample temperature can be eliminated as a possible cause of the observed reduction in projectile neutralization. However, the observed increase of the 1+ charge fraction in the temperature range 650–900 K does correlate strongly with the (2×1)–(1×1) phase transition of the Au(110) surface at 650 K [24,25], at which the ordered ''missing-row'' surface reconstruction is replaced by a more or less random sequence of ''peak'' and ''valleys'' along the [110] direction as shown in Fig. 7. This surface randomization appears to increase the likelihood of close binary encounters, which can terminate the channeling interaction and reduce the total time available for neutralization along a projectile trajectory. The above correlation was confirmed by the experimental observation that at the sample temperature at which the 1+ charge fraction starts its increase, the characteristic channeling pattern seen in the scattered ion angular distribution at low temperature abruptly disappears as has been noted by previous experimental work [26,27]. Although the (2×1)–(1×1) phase transition can dramatically affect the [110] channel, it is expected to have little effect in an arbitrary ''random'' direction, i.e., away from the low-index channels. The temperature dependence of the scattered 1+ charge fraction for projectiles incident along a random direction of Au(110) surface bears out this expectation. As can be seen in Fig. 5, the (2×1)–(1×1) phase transition in this instance has little effect on projectile neutralization.

The 1+ charge fraction was also found to increase with decreasing target temperature below 450 K. The latter increase is attributed to surface contamination during the long cool-down time interval (about 3 h) required for the sample to reach room temperature. After reaching room temperature, a small amount of *C*, estimated to be less than 10% ML, was observed on the Au(110) surface by using electron-induced Auger electron spectroscopy as shown in Fig. 8. There was no detectable *C* in the temperature range 500–900 K. Therefore, it is very possible that the increase of the scattered 1+ charge fraction over the long time interval required for the sample to cool to room temperature is due to additional binary collisions between projectiles and randomly adsorbed *C*. The relatively smaller increase and the larger overall magnitude of the scattered 1+ charge fraction for projectiles incident along the random direction indicates that such binary collisions are already more prevalent along random directions even in the absence of adsorbates present on the surface.

V. SUMMARY

We have measured the temperature dependence of the 1+ charge fraction for 72-keV Ne^{9+} grazingly incident on Au(110). A dramatic increase of the 1+ charge fraction was observed for Ne^{9+} incident along the [110] channeling direction when the sample temperature exceeded 650 K. The accompanying disappearance of the characteristic surface channeling pattern at the same temperature confirms that this decrease in projectile neutralization along the channeling direction is correlated with the (2×1)–(1×1) random phase transition of the Au(110) surface.

Systematic measurements of the dominant scattered projectile charge-state fractions were also made for multicharged He, N, Ne, Na, and Ar ions grazingly incident on a

Au(110) surface. For all projectiles no significant dependence on the primary projectile charge state was found. The main determinant of the neutral and 1+ charge fraction velocity dependence was the neutral binding energy of the projectile in question. For species whose neutral binding energies fell more than 10 eV below the bottom of the Au(110) valence band (He, and Ne projectiles), the apparent 1+ charge fractions were small but finite at very low velocity, and steeply increased once a threshold velocity was reached, which depends on the projectile neutral binding energy, as well as the Fermi energy and work function of the target. The finite low-energy 1+ plateaus were attributed either to resonance ionization of excited states, or, more likely, to possible charge-dependent detection efficiencies for these two species, which are progressively more favorable for the registration of 1+ ions over neutral atoms as the energy is decreased. If the neutral binding energy of the projectile was slightly above the Fermi level (Na), the dominant charge fraction was found to be 1+, while the neutral fraction showed a ''kinematic resonance'' shape as a function of projectile velocity. This resonance behavior was explained by the fact that the neutral fraction reflects the density of occupied states of metal valence-band electrons at the shifted atomic level ''seen by'' the moving projectile. This density of states appears in the projectile rest frame as a kinematically altered Fermi-Dirac distribution, which has a maximum as a function of projectile velocity. Our experimental data were well fitted by Eq. (1) based on the ''kinematic resonance'' model. According to the fitting results, we conclude that the final charge-state distributions are mainly dependent on the competition of resonant ionization and resonant neutralization processes, which are completed when the scattered Na projectiles are still within ~ 3 Å of the surface plane.

Note added in proof. We thank Professor H. Winter for pointing out that the opening of the Auger loss channel, discussed in Sec. III C, has been previously observed by him [28] as a kinematic threshold in the formation of scattered He^+ ions during grazing interactions with Al(111).

ACKNOWLEDGMENTS

We would like to thank J. W. Hale and G. W. Ownby for their skilled technical support. This research was sponsored by the Division of Applied Plasma Physics, Office of Fusion Energy, and by the Division of Chemical Sciences, Office of Basic Energy Sciences of the U.S. Department of Energy under Contract No. DE-AC05-96OR22464 with Lockheed Martin Energy Research Corporation. Q. Yan was supported through a program administered by the Oak Ridge Institute for Science and Education.

[1] B. D'Etat *et al.*, in *Proceedings of the 6th International Conference on the Physics of Highly Charged Ions, Manhattan, Kansas, 1992*, edited by P. Richard, M. Stockli, C. L. Cocke, and C. D. Lin, AIP Conf. Proc. No. 274 (AIP, New York, 1993), p. 592.

[2] Friedrich Aumayr, in *Book of Invited Talks of the XIXth International Conference on the Physics of Electronic and Atomic Collisions, Whistler, Canada, 1995*, edited by L. J. Dubé, J. B. A. Mitchell, J. W. McConkey, and C. E. Brion, AIP Conf. Proc. No. 360 (AIP, New York, 1995), p. 631; H. Kurz, F. Aumayr, HP. Winter, D. Schneider, M. A. Briere, and J. W. McDonald, Phys. Rev. A **49**, 4693 (1994).

[3] M. Grether, A. Spieler, R. Köhrbrück, and N. Stolterfoht, Phys. Rev. A **52**, 426 (1995); N. Stolterfoht, A. Arnau, M. Grether, R. Köhrbrück, A. Spieler, R. Page, A. Saal, J. Thomaschewski, and J. Bleck-Neuhaus, *ibid*. **52**, 445 (1995).

[4] J. Limburg, S. Schippers, I. Hughes, R. Hoekstra, R. Morgenstern, S. Hustedt, N. Hatke, and W. Heiland, Nucl. Instrum. Methods B **98**, 436 (1995); J. Limburg, S. Schippers, I. Hughes, R. Hoekstra, R. Morgenstern, S. Hustedt, N. Hatke, and W. Heiland, Phys. Rev. A **51**, 3873 (1995).

[5] M. A. Briere, D. Schneider, J. McDonald, M. Reaves, C. Rühlicke, G. Weinberg, and D. Knapp, Nucl. Instrum. Methods B **90**, 231 (1994).

[6] F. W. Meyer, S. H. Overbury, C. C. Havener, P. A. Zeijlmans van Emmichoven, J. Burgdörfer, and D. M. Zehner, Phys. Rev. A **44**, 7214 (1991).

[7] H. Winter, Europhys. Lett. **18**, 207 (1992); H. Winter, C. Auth, R. Schuch, and E. Beebe, Phys. Rev. Lett. **71**, 1939 (1993).

[8] F. W. Meyer, L. Folkerts, H. O. Folkerts, and S. Schippers, Nucl. Instrum. Methods B **98**, 441 (1995).

[9] J. Burgdörfer, C. Reinhold, and F. W. Meyer, Nucl. Instrum. Methods B **98**, 415 (1995); C. Lemell, HP. Winter, F. Aumayr, J. Burgdörfer, and F. W. Meyer, Phys. Rev. A **53**, 880 (1996).

[10] L. Folkerts, S. Schippers, D. M. Zehner, and F. W. Meyer, Phys. Rev. Lett. **74**, 2204 (1995); **75**, 983 (1995).

[11] A. Närmann, K. Schmidt, C. Höfner, W. Heiland, and A. Arnau, Nucl. Instrum. Methods B **78**, 72 (1993).

[12] F. W. Meyer, L. Folkerts, and S. Schippers, Nucl. Instrum. Methods B **100**, 366 (1995).

[13] C. A. Keller, C. A. Dirubio, G. A. Kimmel, and B. H. Cooper, Phys. Rev. Lett. **75**, 1654 (1995).

[14] R. Sitzmann and C. Varelas, Nucl. Instrum. Methods **132**, 633 (1976); B. W. Farmery, A. D. Marwick, and M. W. Thompson, in *Atomic Collision Phenomena in Solids* (North-Holland, Amsterdam, 1970), p. 589.

[15] B. Jacquot and M. Pontonnier, Oak Ridge National Laboratory Report No. CONF-9011136, p. 133 (unpublished).

[16] R. Zimny, H. Nienhaus, and H. Winter, Radiat. Eff. Defects Solids **109**, 9 (1989).

[17] H. Winter, Comments At. Mol. Phys. Vol. **26**, 287 (1991).

[18] J. Los and J. J. C. Geerlings, Phys. Rep. **190**, 133 (1990).

[19] R. Zimny, Surf. Sci. **233**, 333 (1990).

[20] H. D. Hagstrum, in *Electron and Ion Spectroscopy of Solids*, edited by L. Fierman, J. Vennik, and W. Dekeyser (Plenum, New York, 1978).

[21] R. Zimny and Z. L. Miskovic, Nucl. Instrum. Methods B **58**, 387 (1991).

[22] K.-H. Krebs, Fortschr. Phys. **16**, 419 (1968).

[23] D. H. Crandall and J. A. Ray, Rev. Sci. Instrum. **46**, 562 (1975).

[24] J. C. Campuzano, M. S. Foster, G. Jennings, R. F. Willis, and

W. Unertl, Phys. Rev. Lett. **54**, 2684 (1985).
[25] J. C. Campuzano, A. M. Lahee, and G. Jennings, Surf. Sci. **162**, 484 (1985).
[26] A. Niehof and W. Heiland, Nucl. Instrum. Methods B **48**, 306 (1990).
[27] W. Hetterich, C. Höfner, and W. Heiland, Surf. Sci. **251/252**, 731 (1991).
[28] H. Winter, Nucl. Instrum. Methods B **78**, 38 (1993).